Factors affecting the pH and electrical conductivity of MgO–ethylene glycol nanofluids

SAHEED A ADIO, MOHSEN SHARIFPUR* and JOSUA P MEYER

Department of Mechanical and Aeronautical Engineering, University of Pretoria, Private Box 0002 Pretoria, South Africa

Abstract. The pH and electrical conductivity are important properties of nanofluids that have not been widely studied, especially with regard to temperature and ultrasonication energy. To study the factors that affect the pH and electrical conductivity of magnesium oxide–ethylene glycol (MgO–EG) nanofluid, the effects of temperature, volume fraction, particle size and ultrasonication energy were investigated. Two different sizes of MgO were dispersed in EG base fluid up to the volume fraction of 3%, and the pH and electrical conductivity were monitored between the temperatures of 20 and 70°C. Characterization by transmission electron microscopy and size analyses revealed the morphology and sizes of the nanoparticle samples. The pH values dropped consistently with the increase of temperature, while electrical conductivity value increased with the increase of temperature. The experimental result showed that the increase in the MgO volume fraction increased both the pH and electrical conductivity values of the MgO–EG nanofluid. There was no recognizable influence of ultrasonication energy density on the pH and electrical conductivity of the nanofluid; therefore, it was concluded that temperature, volume fraction and particle size are the predominant factors affecting both the pH and electrical conductivity of MgO–EG nanofluid within the present experimental conditions.

Keywords. MgO–EG; nanofluid; pH; electrical conductivity; volume fraction; ultrasonication.

1. Introduction

The rheological characteristics of nanofluids dictate their efficient and optimal utilization in heat transfer equipment that involves flow, such as in car radiator,[1] heat pipes,[2] and refrigeration and air conditioning systems.[3] Generally, nanofluids have shown higher thermal conductivity[4,5] and specific heat capacity[6,7] as a result of the containing nanoparticles. However, problem of increase in viscosity with regard to the increase in the volume fraction of nanoparticles[8–10] is major and requires utmost attention. Besides, a balance must be there between the thermal conductivity and viscosity to be able to maximize the potentials of nanofluids for heat transfer applications.[11] Therefore, there is a need to find which volume fraction will be optimum for which nanofluid and which application.

In other words, to minimize the viscosity enhancement in nanofluid systems, it is very important that a stable nanofluid is formulated. To ensure stable nanofluids, a situation where the van der Waals (VDW) force is lower than the force of repulsion between particles; surface active agents (surfactants or dispersants) or electrostatic stabilization have been proposed.[12] In the case of surface active agent, which is a chemical method, there is no unique formula of addition. Therefore, it involves trial and error which may not be sustainable for the different possible combinations of these chemicals. Electrostatic stabilization on the other hand is often achieved by modifying the pH of the nanofluids, which affects the ionic state of the nanoparticle surface.[13,14] The physical preparation method such as ultrasonication assist mechanism is another factor that has significant effect in complementing either of the two stabilization methods.[15]

From the above discussion, pH modification appears to be the most sustainable stabilization method. According to Wamkam et al,[16] understanding of the pH influence on nanofluids may facilitate investigations of fundamental nature of the heat transfer fluids. Numerous efforts have been focused to study the effect of the pH of nanofluids on their heat transfer characteristics. Wamkam et al[16] reported aggregation, precipitation and enhancement in thermophysical properties (viscosity and thermal conductivity) of water-based nanofluids of ZrO$_2$ and TiO$_2$ at pH of isoelectric point (IEP). When the pH value of ZrO$_2$–water nanofluid was modified from the IEP, the nanofluid viscosity enhancement was reduced by ~46% because the aggregate size reduced greatly and the nanofluid samples became stable. Timofeeva et al[17] reported similar

---

*Author for correspondence (mohsen.sharifpur@up.ac.za)

findings that, changing the pH of SiC–water nanofluid from 5.5 to 10.3 resulted in significant drop in effective viscosity enhancement of the nanofluid to the tune of ∼ 34%. Xian-Ju and Xin-Fang[18] showed that an optimal pH value at which nanofluid viscosity is minimum is achievable when they investigated the effect of pH on the viscosity and thermal conductivity of Cu–H_2O and Al_2O_3–H_2O nanofluids. At the optimal pH values of 9.5 and 8.0 for Cu–H_2O and Al_2O_3–H_2O nanofluids, respectively, their results indicated that the nanofluids were stable and had minimum viscosity enhancements for volume concentration between 0.1 and 0.4%. Li *et al*[19] reported that as pH of Cu–H_2O nanofluid is moved away from IEP, the nanoparticles' surface charge increases due to more frequent attacks to the surface hydroxyl groups and phenyl sulphonic group by potential determining ions (H^+, OH^- and phenyl sulphonic group). This leads to the increase in the zeta potential up to the potential at which the dispersion behaviour becomes stabilized. Other similar works have shown that modifying the pH of nanofluid suspension further beyond the IEP have led to the formulation of stable nanofluids.[20–23]

All the above cited literatures are unanimous on the fact that at IEP (point of zero charge on nanoparticles) the nanoparticles will aggregate due to insufficient electrostatic force to overcome the effectiveness of VDW forces of attraction. If the pH changes further away from the IEP, the ionic charge state of the particle surface increases which produces sufficient electrostatic repulsive force that overcomes the VDW forces of attraction. According to the Derjaguin and Landau, Verwey and Overbeek (DLVO) theory, at IEP the total interaction energy barrier (that must be overcome) is at its minimum giving opportunity for the formation of aggregations (resulting from Brownian motion of the nanoparticles). However, when the pH is adjusted to a value much higher than the pH at IEP, the ionic strength increases. As a result, makes it in a much higher interaction energy barrier. At this state, the aggregates present in the suspension will be at minimum size and the suspension becomes stable.[23]

The pH and electrical conductivity are two interrelated phenomena that are linked to the ionic configuration and surface charge of the nanoparticles in suspension.[13,14] In nanofluids, when nanoparticles are dispersed in the base fluid (e.g., water), electrostatic forces become extant and the strength of the electrostatic forces depends on the degree of ionization of the suspension.[24] This process alters the electrical properties of the base fluid due to the interactions with the particle surface charge. The type and strength of particle surface charge are another important characteristic, as they dictate the agglomeration and deagglomeration structures that will be prevalent in the nanofluids.[25] The charge characteristic is also interrelated with the electrical double layer (EDL), electrophoretic mobility and the electrical conductivity of nanofluids. The interplay between the electrical conductivity, EDL and electrophoretic mobility of nanoparticles in nanofluids has been shown to influence the stability and effective viscosity of colloidal suspensions.[26,27] Therefore, the study of electrical conductivity of nanofluids gets even more crucial at this stage in nanofluids research. Presently, a few research has been directed towards understanding the enhancement evolution of electrical conductivity in nanofluids. Sarojini *et al*[28] reported a linear rise in water-based ceramic nanofluids (Al_2O_3, CuO) with increase in the volume fraction and a nonlinear behaviour in water-based Cu nanofluid. Ganguly *et al*[29] reported a linear increment in electrical conductivity of Al_2O_3–water nanofluid with the increase in the volume fraction. Likewise, Modesto-lopez and Biswas[30] on TiO_2 ceramic. The thermal and electrical conductivity of carbon nanotube (CNT) and graphene have also been studied.[31,32] Table 1 gives a summary of the thermophysical properties of different nanofluids available in the open literature. Generally, nanofluid's electrical conductivity predictions have been mostly attempted[28,33] using the model developed by Maxwell.[34] Ohshima's model on counterion condensation[35] is another model that has been used in nanofluids' electrical conductivity predictions.[36]

Table 1. Summary of thermophysical properties of different nanofluids.

Nanofluid	Thermal conductivity (W mK^{-1})	Electrical conductivity (μS cm^{-1})	pH	Particle size (nm)	Volume fraction (%)	Temperature (°C)	References
Al_2O_3–water	0.661	–	8.0	15–50	0.2	25	18
CuO–water	0.679	–	9.5	25–60	0.2	25	18
Al_2O_3–EG	–	10.26	–	80	1	30	28
CuO–EG	–	18.21	–	80	1	30	28
MgO–EG	0.354	–	–	20	5	30	47
Al_2O_3–EG	0.323	–	–	20	5	30	47
MgO–EG	0.328	–	–	60	5	25	48
Al_2O_3–glycerol	–	0.15	4.21	20–30	2	30	49
Al_2O_3–water	–	2.9	5.5	20	0.01	25	50
Al_2O_3–water	0.6812	314	–		8.47	21	51

There are numerous applications of nanoparticles and nanofluids which cut across sciences, biomedical sciences, pharmaceuticals and engineering fields. Specifically in the context of sustainable energy development and thermal management, nanofluids are becoming more essential as the need for efficient thermal management is of utmost importance. The improved thermal properties of nanofluids are key to efficient thermal management in devices such as microelectromechanical systems (MEMS), nanoelectromechanical systems (NEMS), microchips and microprocessors.[37–39] Electrically conductive fluids have usefulness in the manufacture of electrically conducting paint, electrically conducting adhesives[28] and electric field-induced pattern formation in colloids such as in magnetorheological fluid[40] for lubrication, efficient heat transfer and semi-active control of vehicle suspensions.[41] Research, development and implementation of electrospray technology is also an area that is highly dependent on the knowledge of electrical conductivity of colloid.[30] Also, understanding the electrical conductivity evolutions is particularly vital for lab-on-chip and electrophoretic applications, especially for suspensions with thick EDL, which is typical of salt-free medium, such as ethylene glycol (EG) and propylene glycol (PG).[36] Other emerging areas of applications of nanofluids could be: (i) in medicine, for targeted treatment of malignant cells without damaging healthy tissues, (ii) in biomedical, for drug delivery for some special cases and (iii) in surgery in order to increase the chances of survival of patients.[42–46]

As discussed earlier, stability can be achieved with pH modification which is usually monitored by measuring the zeta potential.[19] Surprisingly, in manipulating the pH value, the temperature to which the nanofluids will be subjected was not always considered. As zeta potential is very sensitive to pH change[19] and nanofluid is meant for high temperature applications, it is expedient to study the pH and electrical conductivity characteristics at elevated temperature. This will further bolster the study of stability of nanofluids. Magnesium oxide (MgO) nanoparticles dispersed in EG was shown to be one of the nanofluids with a very high thermal conductivity and possessing one of the lowest viscosity enhancements.[47] Therefore, this work is aimed at studying the combined influence of temperature, particle size, volume fraction and sonication energy on the pH and electrical conductivity of MgO–EG nanofluid with the intension of providing data for future studies on electrostatic stabilization of the nanofluid.

2. Experimental

2.1 *Materials and equipment*

MgO with sizes estimated by the respective manufacturer as 20 and 100 nm were used in this study and for the sake of simplicity and identification they will be referred to as MgO-20 and MgO-100, respectively. MgO-20 was procured from the US Research Nanomaterial Inc. and MgO-100 was procured from Nanostructured Amorphous Inc. All the nanoparticles have true density of 3.58 g cm^{-3}. In this experimental study, EG used as the base fluid was obtained from Merck Millipore, South African branch, with 99.5% purity and pH of 6–7.5.

A digital Highland HCB1002 (max: 1000 g and accuracy of $\pm$ 0.01 g) weighing balance was used to measure the samples during preparation. Ultrasonic vibration was achieved with a 24 kHz, 200 W Hielscher ultrasonicator (UP200S) with a 12 mm stainless-steel probe. LAUDA ECO RE1225 Silver constant temperature thermal bath was employed to control the temperature of nanofluid samples during measurement from 20 to 70°C. The pH measurement was accomplished using Jenway 3510 pH meter with –2 to 19.999 pH measurement range and $\pm$ 0.003 pH measurement accuracy. The probes are the multipurpose glass body combination electrode and an automatic temperature compensation (ATC) probes. The electrical conductivity meter (CON700) used in this study was manufactured by EUTECH Instrument and has $\pm$ 1% measurement accuracy. A 2-cell electrical conductivity probe equipped with an internal ATC and cell constant $k = 1.0$ was supplied with the equipment.

2.2 *Nanofluids' characterization and preparation*

The size and morphology characterization were carried out using transmission electron microscope (TEM). The nanoparticles were dispersed in acetone so that the rapid drying method could be employed for the TEM captures.[16] The TEM device was JEOL JEM-2100F which operated at 20 kV. X-ray diffraction (XRD) patterns of the nanoparticle samples were obtained using XPERT-PRO X-Ray Diffractometer manufactured by PANalytical BV, Netherlands. The XRD characteristics were taken using cobalt cathode radiation source at 35 kV, 50 mA, step size of 0.001°, time step of 12.705 s, and recorded between 5° and 90°.

Two-step method[52] was employed to prepare the nanofluids' samples with ultrasonication for proper homogenization. The homogenization process was carried out in a 100 ml beaker and placed in the thermal bath during preparation due to the high energy impact of the process. For each volume fraction, the equivalent mass of nanoparticles was determined using the mass and densities of the base fluid and the nanoparticles as

$$\phi = \frac{v}{V} = \frac{m_{MgO}/\rho_{MgO}}{m_{MgO}/\rho_{MgO} + m_{EG}/\rho_{EG}}, \tag{1}$$

where ϕ is the volume fraction, v the volume of the nanoparticles, V the volume of nanoparticles plus base fluid, m the mass, and ρ the density. Zeta potential (ζ) of the

nanofluid samples were measured using Zetasizer nano ZS (Malvern Instrument Inc., London, UK). The equipment measures the electrophoretic mobility of the particles using capillary cells with electrodes at either ends to which electric potential is applied. The measured electrophoretic mobility of the particle is then used to calculate the ζ potential using Henry's function. The ζ potentials were measured at room temperature (25°C) with applied voltage of 10 V. The pH of the sample was adjusted using 0.5 M KOH and HCl, and the experiment was repeated at least 4 times in order to calculate the average of them. The measurement was run at $V = 10$ V and $T = 25$°C, due to the equipment limitation, a very dilute concentration of 0.05% was measured while higher concentrations were not suitable.

2.3 Measurement details

The calibration of the pH metre was performed at 2 points at 25°C using buffer solutions with pH values of 7 and 10. The electrical conductivity metre was calibrated with a 1413 μS cm^{-1} standard calibration fluid (supplied by Jenway) at 25°C. After calibration, measurements made by both devices gave less than 1% deviation from the respective values of the standard solutions. A water jacketed sampling unit with two cups was manufactured in-house to hold samples and for ease of temperature control during measurement. The schematic of the experimental set-up is shown in figure 1. The samples are manually stirred until the temperature and the measurement values are stable. Both metres are equipped with slope monitor, which gives indication when the measurement does not vary between 0.005 and 0.01 for pH and electrical conductivity metres, respectively.

3. Results and discussion

3.1 Nanoparticles' physical characterization

The results of the TEM capture for the MgO-20 and MgO-100 nanoparticles are shown in figure 2. The nanoparticles' morphology is polyhedral, which corresponds to the manufacturer's estimation. In figure 2a, the size distribution of the nanoparticle is narrow and a representative of manufacturer's quoted size (figure 3). Figure 2b represents the MgO-100 nanoparticles and according to the size analysis presented in figure 3, the average size falls within the manufacturer's quoted size of 100 nm.
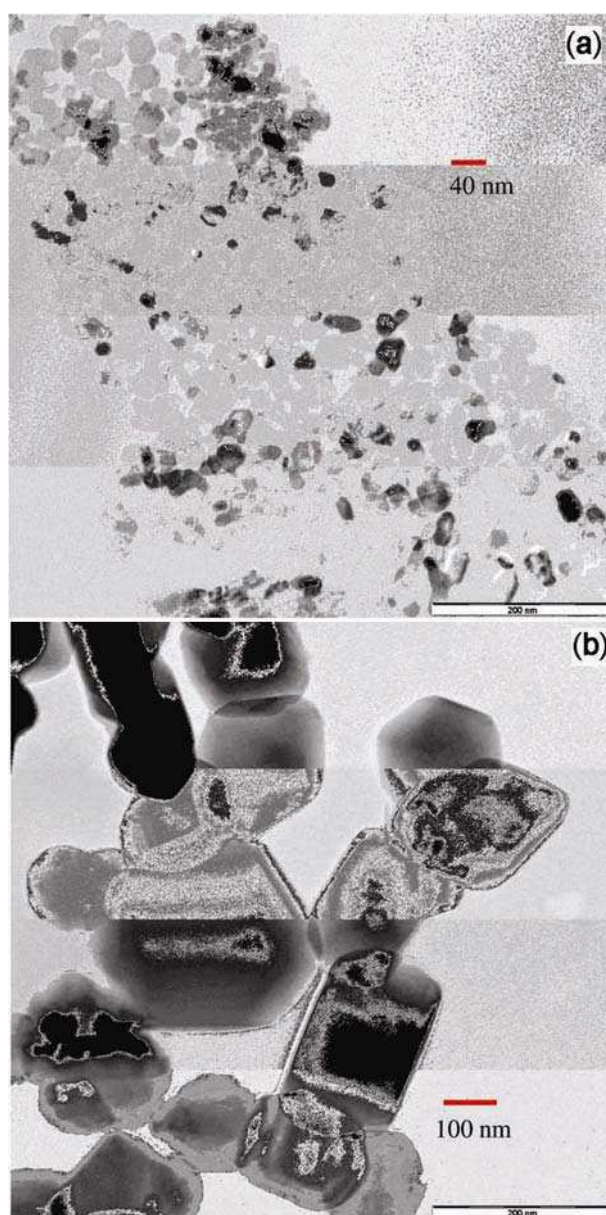
Figure 2. TEM image of MgO nanoparticles: (**a**) MgO-20 and (**b**) MgO-100.

Figure 1. Schematic of the experimental set-up with inset showing the pictographic of the measurement site.

In figure 4, the XRD of the MgO nanoparticles is presented alongside with the energy-dispersive spectroscopy (EDS) patterns. The patterns' major peaks correspond to Periclase structure (MgO) from the Joint Committee on Powder Diffraction Standards (JCPDS) database (card number: 01-078-0430). The peaks *hkl* lattice parameters showed that the MgO has cubic crystal system with Fm3-fm spacing group and agrees with the previously published result of Mastuli *et al.*[53] Other peaks in MgO-20 as shown in figure 4a with shaded circles are identified with Brucite ($Mg(OH)_2$) having an hexagonal structure. The corresponding EDS graphs also confirm that major constituents of the samples are magnesium and oxygen. When the XRD patterns were compared with those provided by the manufacturers (not shown here), they gave good agreement. However, there is a 5–10° shift in 2θ position in the present experimental results, which is due to the fact that cobalt ($\lambda = 1.789$ Å) was used as X-ray source in this work, while copper ($\lambda = 1.59$ Å) was used by the respective manufacturers. Applying the Scherrer equation (equation 2) can estimate the average crystallite size by measuring the broadening of the XRD peaks. The equation predicts the crystallite size with $\pm 10\%$ deviation.[55] For the present experiment, the predicted average crystallite sizes are ~ 18 and 43 nm for MgO-20 and MgO-100 nanoparticles, respectively.

$$d = \frac{k\lambda}{\beta \cos\theta}, \qquad (2)$$

where *d* is the crystallite size of the nanoparticle, *k* a constant, λ the wavelength of irradiation, β the full-width
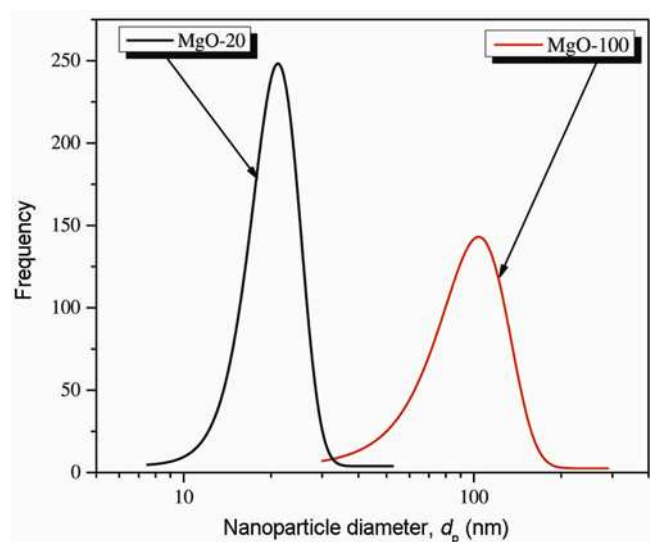
Figure 3. MgO nanoparticles size distribution.
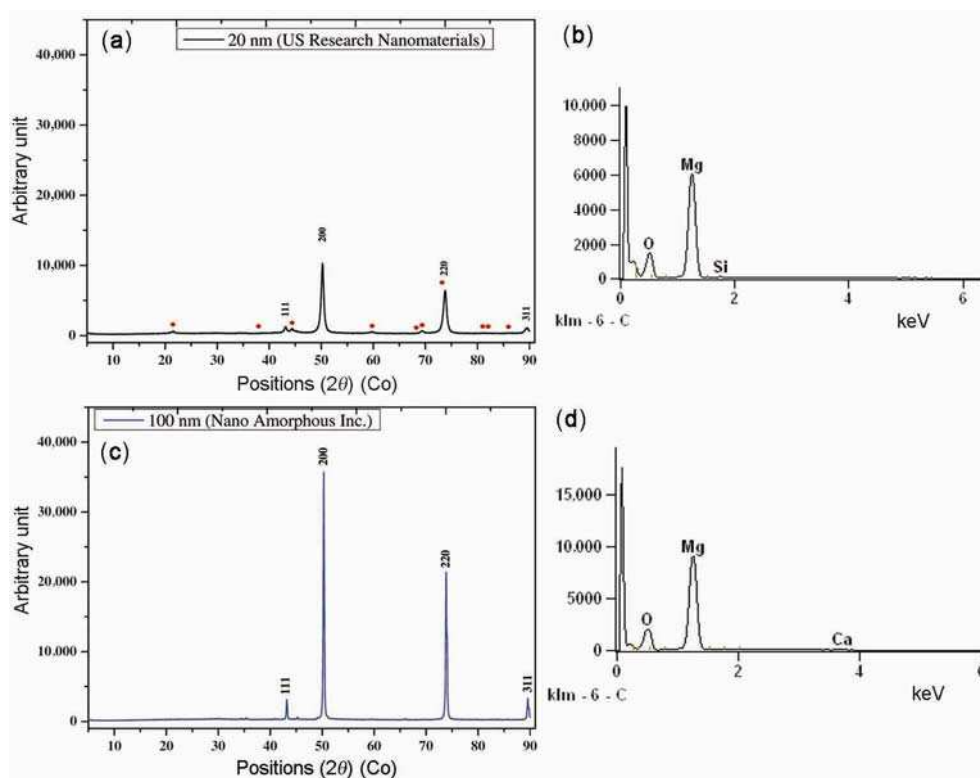
Figure 4. XRD and EDS spectral patterns of MgO nanoparticles: (**a** and **c**) XRD spectral of MgO-20 and MgO-100 nm, respectively and (**b** and **d**) EDS spectral of MgO-20 and MgO-100 nm, respectively.

half-maximum (FWHM) of prominent peaks and θ half of the peak position (i.e., θ is half of 2θ).

The starting pH values of the nanofluid samples from MgO-20 and MgO-100 at 0.05% volume fraction were 9.27 and 8.5, respectively. The initial ζ potential was measured before titrating with KOH and HCl, after which the ζ potential was measured. Figure 5 shows the variation of the ζ potential with pH adjustment. The initial ζ potentials of the samples are well within the stable region (± 30 mV) and with the pH modification IEP was observed between pH 10 and 11 for both samples. The inset of figure 5 shows the behaviour of the sample after 5 days of preparation for the initially prepared samples and that at pH close to IEP. It can be seen that the samples used in this experiment are stable, as there was little or no sedimentation even without pH modification or surfactant addition.

3.2 *Experimental uncertainty*

The measurement errors relating to the variables in the preparation, pH, electrical conductivity, and temperature measurements form the basis for the uncertainty in this work. The weighing balance was used to measure in the range of 0–100 g with uncertainty of $\pm 0.01\%$. For the pH and electrical conductivity measurements, their uncertainties were ± 0.015 and $\pm 1\%$, respectively, at device full range. The thermocouples for both the pH metre and electrical conductivity metre measured temperature in the range of 20–70°C with individual uncertainty of $\pm 0.56\%$.

3.3 *Influence of temperature on pH and electrical conductivity*

The pH of a solution can change with temperature, due to the effect of temperature on the dissociation of weak

Figure 5. Zeta potential (ζ) of MgO–EG nanofluids as a function of pH modified by KOH and/or HCl.

acids' and bases' groups, and the splitting of water component into H^+ and OH^-. Figure 6 presents the influence of temperature on the pH of MgO–EG nanofluid at various volume fractions alongside with the base fluid. The pH of the base fluid measured at 25°C was 6.78, which gave a good agreement with the manufacturer's reference value (i.e., 6–7.5) and also the value reported by Timofeeva *et al*[50] (i.e., 6.8). Table 2 shows the measured pH and electrical conductivity of EG and of nanofluid samples at room temperature and 2.183×10^6 kJ m^{-3} suspension energy density. The presence of MgO gave approximately 60 and 53% enhancement in the pH value for MgO-20 and MgO-100, respectively, at 3% volume fraction. However, these values reduced with the increase in temperature. The trends as presented in figure 6 show significant reduction in the pH values between 20 and 70°C temperatures that were investigated. Similar results were published by Konakanchi *et al*[24] on propylene glycol/water (60 : 40) based nanofluids for Al_2O_3, SiO_2 and ZnO. Figure 6 shows the results of MgO–EG sonicated for 30 min (corresponding with energy density 2.183×10^6 kJ m^{-3}); however, very similar trends have been found for other sonication times (60 min corresponds with 4.364×10^6 kJ m^{-3} and 180 min corresponds with 13.092×10^6 kJ m^{-3}), indicating that ultrasonication time/energy does not attenuate this trends. The fact that temperature variation affects the value of pH of the MgO–EG nanofluid, which is not the case for the base fluid, tells the significance of this research on stability of the nanofluid. It was also indicated in the introduction part that pH was shown to affect the zeta potential,[19,55] which is used to measure the stability of nanofluids.

The behaviour of the electrical conductivity of EG investigated in the present work is somewhat similar to the pH measurement with value changing from 0.11 to 0.35 μS cm^{-1} (figure 6). At room temperature the electrical conductivity value of the EG used in this experiment was 0.11 μS cm^{-1}, which totally disagree with the 1.07 μS cm^{-1} reported by Sarojini *et al*[28] but comparable to the value of other glycol.[36] The reason for this disparity could lie in the purity of the EG used in these two experiments. In the present experiment, the EG had 99.5% purity while Sarojini *et al*[28] did not provide the detail of the purity of their EG base fluid. Although EG is
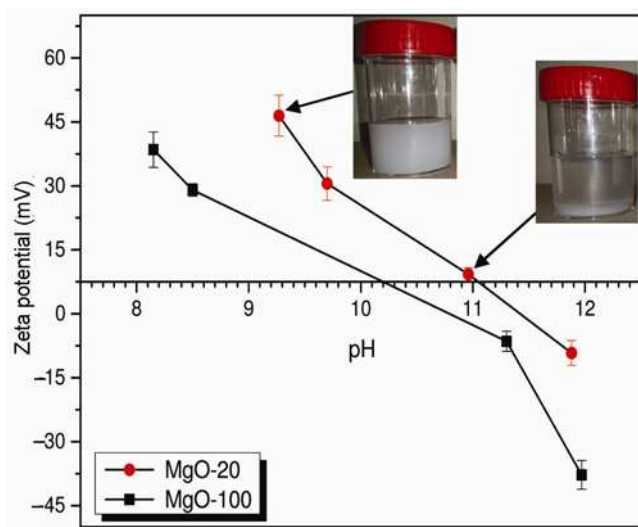
Table 2. Experimental values of the pH and electrical conductivity of EG and MgO-20 nanofluid at 25°C.

Volume fraction, ϕ (%)	Electrical conductivity, K (μS cm^{-1})	pH
EG	0.1133	6.78
0.1	3.01	9.66
0.5	6.68	10.14
1.0	8.73	10.33
2.0	11.74	10.3
3.0	14.05	10.84

mildly polar, it is also highly hygroscopic; therefore, if it is overexposed to the atmosphere it will absorb moisture, thus alter the purity and also water is a polar liquid,[28] which means moisture will increase the electrical conductivity value.

The apparently unchanging values of the pH and electrical conductivity of the base fluid with temperature further supports the fact that the pH and electrical conductivity are two interrelated processes, which are linked by ionic concentration/activity. In figure 7, the plots of the effective electrical conductivity of MgO–EG nanofluid against temperature at various volume fractions are presented. The addition of MgO nanoparticles up to 3% by volume to EG displayed a significant increase in the electrical conductivity. The influence of temperature is also significant as the electrical conductivity increased with the increase in sample temperature. The graph of MgO-20 in figure 7a shows that there is electrical conductivity saturation at 2% through 3% volume fractions and around 40–70°C which is not the case with MgO-100 in figure 7b. This is the volume fractions at which counterion condensation (i.e., saturation of electrical conductivity determining ions) was noticed and as the temperature increased the trend remained and became more pronounced. Counterion condensation will be further discussed in the next section. In figure 8, the electrical conductivity values are normalized in order to study the increment behaviour of the electrical conductivity of MgO–EG relative to the base fluid within the experimental temperature range. Increasing the temperature up to 30°C caused the increase of relative electrical conductivity to a maximum value and further increment in the temperature gave a
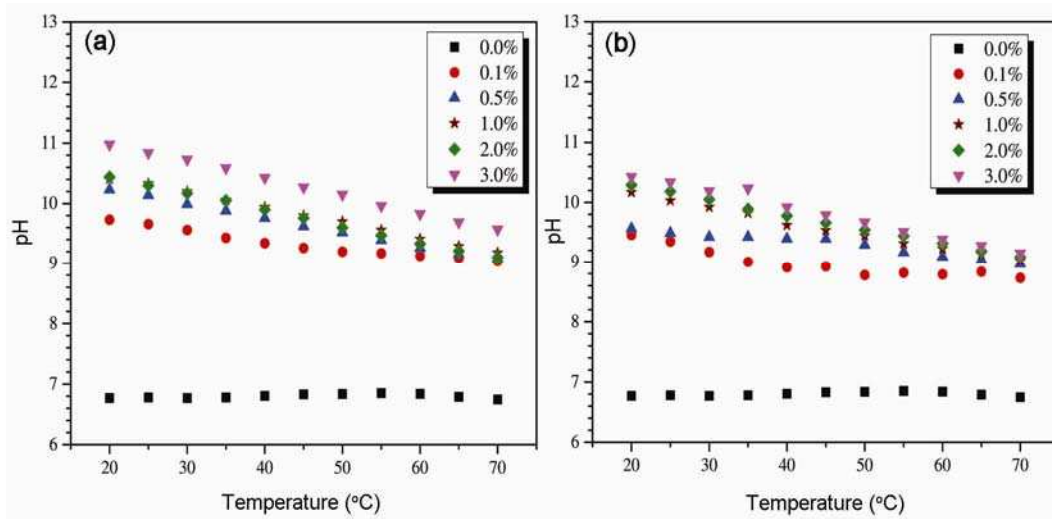
Figure 6. Influence of temperature on the pH of MgO–EG nanofluid: (**a**) MgO-20 and (**b**) MgO-100.
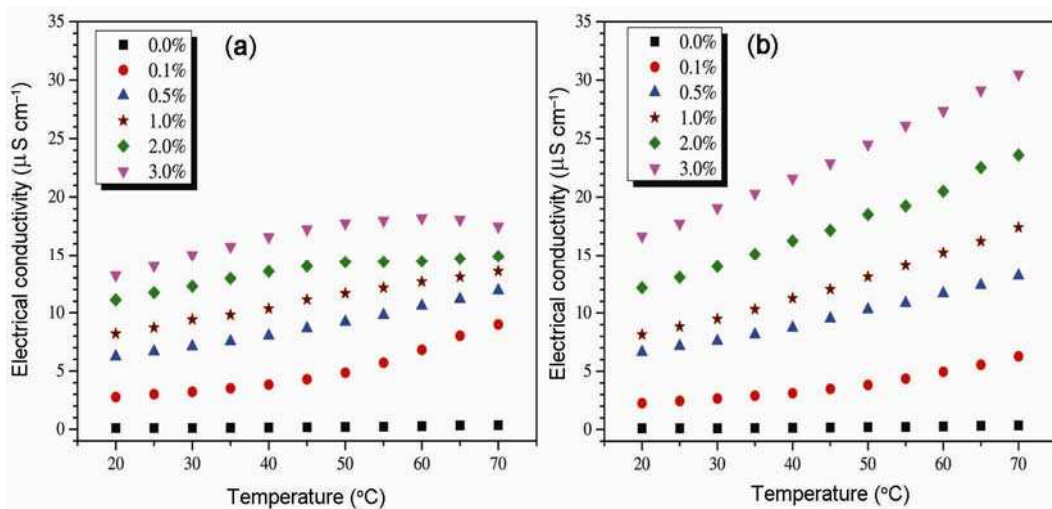
Figure 7. Influence of temperature on the electrical conductivity of MgO–EG nanofluid: (**a**) MgO-20 and (**b**) MgO-100.

continual drop in the relative electrical conductivity. This shows that the per cent (%) increment in the electrical conductivity of base fluid as temperature is higher than the % increment in the MgO–EG nanofluids. For the base fluid a 218.2% increment was recorded, while about 40% increment was recorded for 3% MgO-20 between 20 and 70°C. Consequently, the normalized electrical conductivity reduced as the temperature increased. MgO is widely used as electrical insulators in technical devices such as thermocouples, coaxial heating elements and electrical cables, especially in the temperature region below 1000 K.[56,57] Therefore, the relative electrical conductivity plot in figure 8 depicted an electrically insulating nanofluids as the temperature increases. The graphs of the relative pH against temperature, which is presented in figure 9, show comparable behaviour as noted for

electrical conductivity; the values reduced with the increase in the nanofluid temperature. Similar results on the pH for other types of nanofluids were reported recently by Konakanchi *et al.*[24]

3.4 *Effect of volume fraction and size on pH and electrical conductivity*

As shown in figures 10 and 11, increasing the volume fraction with the addition of MgO nanoparticles significantly increased the electrical conductivity and pH values with regard to the base fluid. In figure 10, the relative electrical conductivities for all the samples of MgO–EG nanofluids with respect to the volume fraction show that there is significant enhancements in the electrical conductivity values even at the low MgO volume fraction of 0.1%.
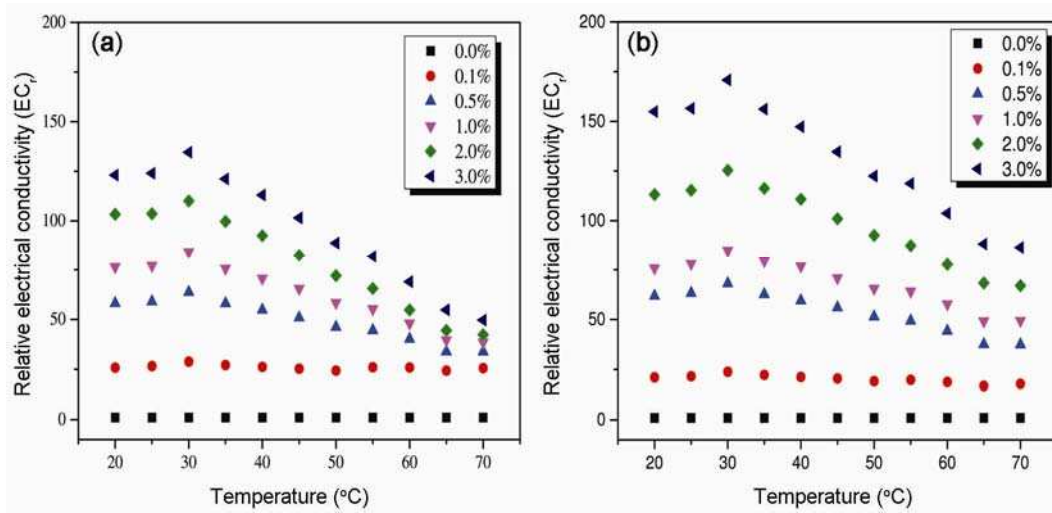
Figure 8. Relative electrical conductivity of MgO–EG nanofluid against temperature: (**a**) MgO-20 and (**b**) MgO-100.
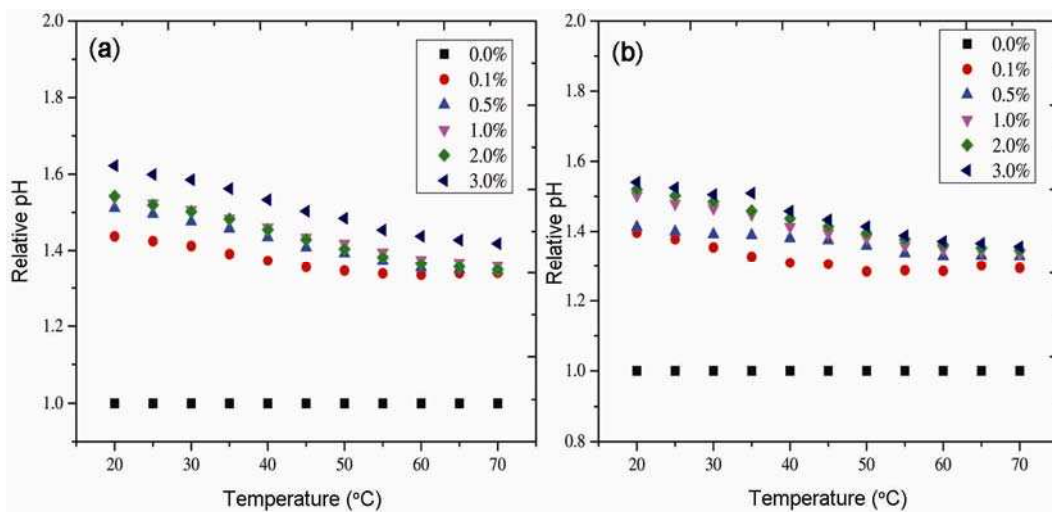
Figure 9. Relative pH of MgO–EG nanofluid against temperature: (**a**) MgO-20 and (**b**) MgO-100.
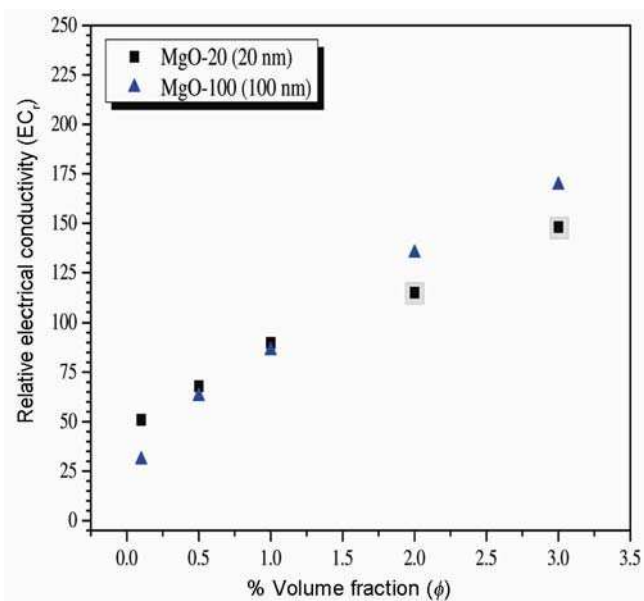
Figure 10. Effect of the volume fraction on the relative electrical conductivity of MgO–EG at room temperature.
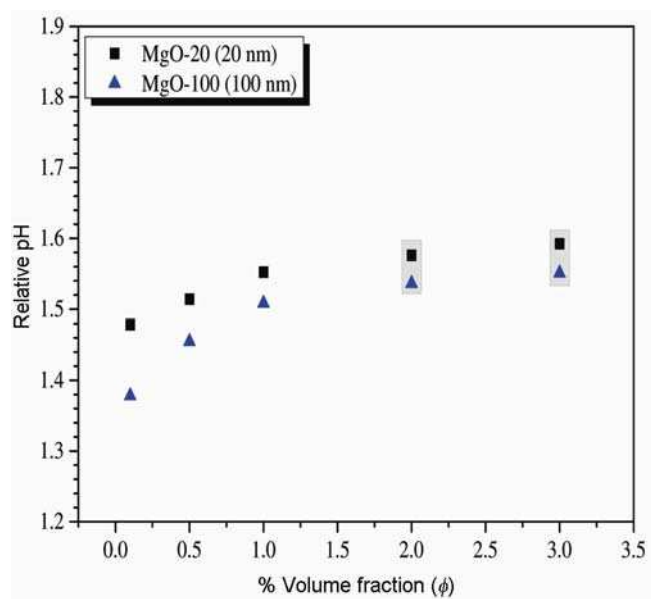
Figure 11. Effect of the volume fraction on the relative pH of MgO–EG at room temperature.

The enhancement increases with the increase in the volume fraction of MgO. Clearly in figure 10, the effect of MgO particles size does not have a definitive pattern on the electrical conductivity of these nanofluids. This trend is unlike those reported by Sarojini *et al*[28] on Al₂O₃–water nanofluid and White *et al*[36] on Al₂O₃–PG nanofluid. The electrical conductivity of the MgO-20 was initially slightly higher than that of MgO-100 with the latter trends suggesting the presence of counterion condensation[30,36] and it is more pronounced in the MgO-20 particles as highlighted with shaded bars in figure 10.

Usually in a salt-free suspension such as MgO–EG nanofluid, there are no ions different from the ones stemming from the suspended particles which allow for the formation of thick EDL, because of the low ionic strength of the suspension. In this type of system the ionic conductivity in the EDL is typically greater than the bulk conductivity, so that the surface conductance increases the effective electrical conductivity of the suspension.[58] There exists a critical particle surface charge density beyond which the surface conductivity has no appreciable influence on the electrical conductivity of the suspension. Therefore, as the volume fraction increases this adds to the total charge present and the electrical conductivity increases until the critical surface charge density is reached. Further increment in the volume fraction only increases the amount of counterions, which feeds the condensation regions (regions close to the particle surface) and leaving the bulk charge and potential virtually unchanged, thereby reducing the electrical conductivity incremental slope or sometimes cause the electrical conductivity to plateau.[36,59] Regarding the effect of size of nanoparticles on the pH, the relative pH plot of figure 11 shows that the smaller the particle size, the higher the pH value. The shaded rectangles in figure 11 correspond with those in figure 10 at the point of counterion condensation. Contrary to the works of Minea and Luciu[60] and Ganguly *et al*[29] which reported 379.6 and 833% enhancement in electrical conductivity for alumina nanofluids at 4 and 0.5% volume fractions, respectively, the percentage enhancement in the present investigation is as high as ~ 6000% at 0.5% volume fraction and 25°C. The high enhancement value recorded compared to past works is probably due to the different nanoparticle types, base fluids and nanoparticles' size.

3.5 *Electrical conductivity and pH at different ultrasonication times*

The influence of ultrasonication time on the electrical conductivity and pH of MgO–EG nanofluid is shown in figure 12 for MgO-20 nanoparticles. Although ultrasonication energy density applied for the preparation of the nanofluids changes the electrical conductivity and pH values, as observed from the experimental data, however, ultrasonication appears not to have a specific pattern or relationship with these thermophysical properties. Similar results were obtained for MgO-100 nanoparticles. The nonmonotonic trend with ultrasonication energy density suggests complexity in the nanofluid system. Therefore, the particle volume fraction, temperature and size seem to be the predominant factors that has recognizable relationship with the pH and electrical conductivity of MgO–EG nanofluid.

3.6 *pH and electrical prediction with existing models*

In recent times a combined empirical correlation was proposed by Konakanchi *et al*[24] for the prediction of the
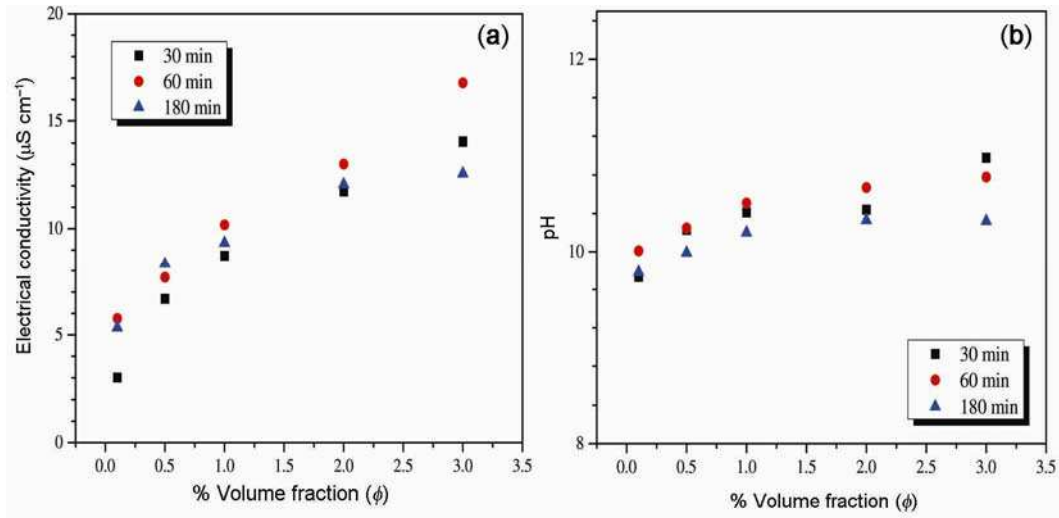
Figure 12. Influence of ultrasonication time/energy density on the electrical conductivity and pH of MgO–EG nanofluid at 20°C: (**a**) electrical conductivity and (**b**) pH.

pH of nanofluids. They considered the nanofluid temperature, volume fraction and nanoparticle size to arrive at the empirical model below

$$\frac{pH_{nf}}{pH_{bf}} = \left[a_1 \left(\frac{T}{T_0} \right)^2 + a_2 \left(\frac{T}{T_0} \right) + a_3 \right]$$

$$\times \left[b_1 \phi^2 + b_2 \phi + b_3 \right] \left[c_1 \left(\frac{d}{d_0} \right)^2 + c_2 \right], \quad (3)$$

where T_0 and d_0 are reference temperature and particle size taken to be 273 K and 100 nm, respectively. a_1–a_3, b_1–b_3 and c_1, c_2 are all empirical constants obtainable from regression analysis.

Regarding the prediction of electrical conductivity, Maxwell's model on conductivity was applied to the electrical conductivity of aluminium oxide ceramic suspensions.[33] Cruz *et al*[33] prepared their suspension using 520 nm alumina in distillated water up to 35% volume fraction. They applied both NH_4Cl and HCl to modify the ionic strength and pH of the suspension, respectively. Maxwell's equation was also successfully applied to experimental data by Turner[61] to predict and explain the behaviour of electrical conductivity of suspension of particles fluidized by $NaCl_{aq}$ solution. The model predicts the conductivity of liquid–particles system such as nanofluids as a function of the individual conductivities of the suspension components (particle and base fluid) and the volume fraction of the dispersed phase (particle) such that

$$\frac{K_{nf}}{K_{bf}} = 1 + \frac{3(\alpha - 1)\phi}{(\alpha + 2) - (\alpha - 1)\phi}, \quad (4)$$

where α is K_{nf}/K_{bf}, K_{bf} is the electrical conductivity of the base fluid, K_p the electrical conductivity of the

nanoparticles, K_{nf} is the electrical conductivity of the nanofluid. Maxwell's model is valid for low volume fraction with the assumption that particles are randomly distributed and at distances significantly larger than their sizes. Generally, Maxwell theory on conductivity evolves depending on the conducting nature of the dispersed phase[33] according to the following approximations:

(i) if dispersed phase is an insulating type (i.e., $k_p \ll k_{bf}$), equation (4) is approximated as

$$\frac{k_{nf}}{k_{bf}} = 1 - \frac{3}{2}\phi.$$

(ii) if dispersed phase has equal conductivity with the base fluid, then equation (4) is

$$\frac{k_{nf}}{k_{bf}} = 1.$$

(iii) if the dispersed phase is conducting particles (i.e., $k_p \gg k_{bf}$), equation (4) is approximated as

$$\frac{k_{nf}}{k_{bf}} = 1 - 3\phi.$$

The bulk electrical conductivity of MgO is reported as 10^{-14} μS cm^{-1} in the literature.[63] This value is much lower than the measured electrical conductivity of EG (0.11–0.35) in the present experimental temperature range, which suggests that the effective electrical conductivity of the nanofluids will be best predicted using the first approximation of Maxwell's equation above. However, the first approximation of equation (4) falls short in predicting the behaviour of the electrical conductivity, as the model is predicting insulation behaviour against particle volume concentration while the experimental

data showed enhancement in the values of the electrical conductivity of the nanofluid with respect to the increase in the nanoparticle volume fraction. Maxwell's model[34] failed to predict the electrical conductivity of the present nanofluid and other nanofluids in the past[29,60] because the model was developed considering only the physical properties such as the densities and bulk conductivities of suspension constituents. A realistic electrical conductivity model must take into consideration nanoparticles size alongside with nanoparticle surface charge, neither of which is accounted for in the Maxwell model. The combined effects of surface charge (ionic concentration) and particle size are usually expressed as electrokinetic radius, κa, where κ is a function of ionic strength of the suspension, known as the inverse of Debye length and a is the particle radius. The electrical conductivity of nanofluids is described with a complex dependence on nanoparticles loading, temperature, particle size and electrokinetic phenomenon such as; EDL characteristics, electrophoretic mobility, ion and counterion concentrations which are not considered in the formation of most standard models.[29,60] Although some of these factors have been considered to develop different analytical expressions for the calculation of electrical conductivity of colloids in the past.[63–65] However, these expressions are formulated for concentrated suspension of spherical particles in electrolyte solution (i.e., suspensions containing ions other than counterions) and are not presented in a form that can be easily compared with experimental data such that the authors used simulated values to test their models.

Ohshima[35] developed an analytical expression for the computation of the electrical conductivity based on Kuwabara's cell model[66] and applicable for dilute suspension in a salt-free medium such as the case investigated in this paper. He reported two limiting cases in which, (i) electrical conductivity increases linearly with the increase in the volume fraction and the (ii) electrical conductivity increases slowly or is constant and independent of the volume fraction increase due to the effect of counterion condensation. A critical zeta potential (ζ_c) is the point below which the electrical conductivity increase linearly with the volume fraction and above which counterion condensation effect is observed[36] and it is defined as

$$\zeta_c = \frac{kT}{ze}\ln(1/\phi). \tag{5}$$

For limiting case (i), $\zeta < \zeta_c$:

$$K_{nf} = \frac{3ze\varepsilon_r\varepsilon_0\zeta}{4\pi a^2\lambda}. \tag{6}$$

For limiting case (ii), $\zeta \geq \zeta_c$:

$$K_{nf} = \frac{3e\varepsilon_r\varepsilon_0 kT}{a^2\lambda}\phi\ln(1/\phi), \tag{7}$$

where λ is the counterion drag coefficient[67] given as

$$\lambda = \frac{N_A e^2 |z|}{\Lambda_c^0}. \tag{8}$$

The parameters k is the Boltzmann constant, T the absolute temperature, ε_r the relative permittivity, ε_0 the permittivity of vacuum, z the valence of the particle, e the elementary charge, a the particle radius, N_A Avogadro's number, and Λ_c^0 the limiting ionic conductance. Following the procedure outlined by White *et al*[36] either of equation (6) or (7) could not be fitted into our experimental data. The critical ζ_c calculated from equation (5) is 88.7 mV for 0.1% volume fraction, 68.0 mV for 0.5%, 59.1 mV for 1%, 50.2 mV for 2% and 45.0 mV for 3%. The ζ potential measured for the EG-based MgO nanofluids without the addition of any pH modifier is approximately 47.0 and 30.0 mV for MgO-20 and MgO-100, respectively (presented in figure 5). The ζ potential of the MgO-20 falls in limiting case (i) up to 2% and limiting case; and (ii) at higher volume fraction which also correspond to the volume fraction of counterion condensation. For MgO-100 the measured ζ potential falls in the limiting case (i).

Using equation (3), regression analysis was performed to fit the present pH experimental data. Figure 13 shows the parity plot of the predicted relative pH against the experimental relative pH values with 95% confidence interval. The regression analysis based on equation (3) running close to a million iteration and 0.00001 iteration convergence criterion for the present pH data was fitted with regression coefficients a_1, a_2, a_3, b_1, b_2, b_3, c_1 and c_2 as −0.19, −0.074, 1.205, 199.068, −0.066, −2.368, 0.037 and −0.687, respectively. With the plot of figure 13, it can
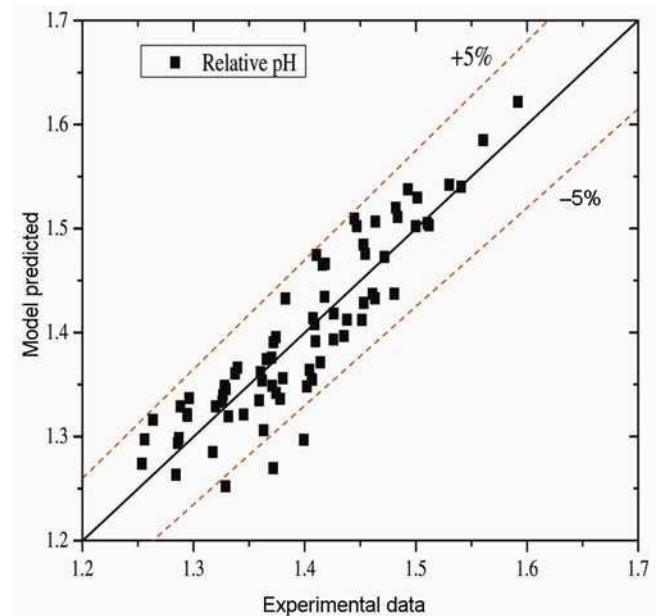
Figure 13. Parity plot between the predicted and experimentally measured pH data.

be said that the equation in form of equation (3) is well suited for the prediction of the present experimental data.

4. Conclusion

This paper presents the results of the experimental measurements on the pH and electrical conductivity behaviours of MgO–EG nanofluid with respect to temperature variation, nanoparticles size, volume fraction and ultrasonication time/energy. Three different sizes of MgO nanoparticles were dispersed in EG using ultrasonication-assisted two-step method. The experimental results indicate that the pH and electrical conductivity of the nanofluid samples are significantly greater than the base fluid values. The pH and electrical conductivity increments are functions of the temperature, volume fraction and particle size. At room temperature, minimum electrical conductivity and pH enhancements of $\sim 6000\%$ and $\sim 50\%$, respectively, were observed for a volume fraction of 0.5%. The electrical conductivity increment does not follow a linear curve with respect to the increase in the nanoparticle volume fraction which suggests counterion condensation. Both the pH and electrical conductivity of the nanofluid increased with reduction in particle size. However, ultrasonication time/energy does not show any recognizable relationship with the measured values of the electrical conductivity and pH of MgO–EG nanofluid samples. Therefore, only temperature, volume fraction and nanoparticle size showed distinct pattern with the MgO–EG nanofluids regarding the thermophysical properties investigated.

The significance of the effect of temperature variation on the pH of nanofluid will be on the stability of the nanofluid, as the ζ potential of nanofluids is very sensitive to changes in pH. Summarily, pH and electrical conductivity are two properties of nanofluid that are linked to the stability of nanofluids.

Acknowledgement

References

1. Peyghambarzadeh S M, Hashemabadi S H, Jamnani M S and Hoseini S M 2011 *Appl. Therm. Eng.* **31** 1833
2. Zamzamian A, Oskouie S N, Doosthoseini A, Joneidi A and Pazouki M 2011 *Exp. Therm. Fluid Sci.* **35** 495
3. Mahbubul I M, Khaleduzzaman S S, Saidur R and Amalina M A 2014 *Int. J. Heat Mass Transf.* **73** 118
4. Chandrasekar M, Suresh S and Bose A C 2010 *Exp. Therm. Fluid Sci.* **34** 210
5. Godson L, Raja B, Lal D M and Wongwises S 2010 *Exp. Heat Transf.* **23** 317
6. Kumaresan V and Velraj R 2012 *Thermochim. Acta* **545** 180
7. Nieh H-M, Teng T-P and Yu C-C 2014 *Int. J. Therm. Sci.* **77** 252
8. Żyła G, Witek A and Cholewa M 2013 *J. Exp. Nanosci.* **10** 1
9. Kole M and Dey T K 2011 *Int. J. Therm. Sci.* **50** 1741
10. Rashin M N and Hemalatha J 2013 *Exp. Therm. Fluid Sci.* **48** 67
11. Prasher R, Song D, Wang J and Phelan P 2006 *Appl. Phys. Lett.* **89** 1
12. Yu W and Xie H 2012 *J. Nanomater.* **2012** 1
13. Lee D, Kim J and Kim B 2006 *J. Phys. Chem. B* **110** 4323
14. Degen A and Kosec M 2000 *J. Eur. Ceram. Soc.* **20** 667
15. Ghadimi A and Metselaar I 2013 *Exp. Therm. Fluid Sci.* **51** 1
16. Wamkam C T, Opoku M K, Hong H and Smith P 2011 *J. Appl. Phys.* **109** 024305
17. Timofeeva E V, Smith D S, Yu W, France D M, Singh D and Routbort J L 2010 *Nanotechnology* **21** 215703
18. Xian-Ju W and Xin-Fang L 2009 *Chin. Phys. Lett.* **26** 1
19. Li X F, Zhu D S, Wang X J, Wang N, Gao J W and Li H 2008 *Thermochim. Acta* **469** 98
20. Li X, Zhu D and Wang X 2007 *J. Colloid Interface Sci.* **310** 456
21. Huang J, Wang X, Long Q, Wen X, Zhou Y and Li L 2009 *Symposium on photonics and optoelectronics* (Wuhan: IEEE eXpress Conference Publishing) p 1
22. Wang X, Li X and Yang S 2009 *Energy Fuels* **23** 2684
23. Younes H, Christensen G, Luan X, Hong H and Smith P 2012 *J. Appl. Phys.* **111** 064308
24. Konakanchi H, Vajjha R S, Chukwu G and Das D K 2014 *Heat Trans. Eng.*
25. Prasher R, Evans W, Meakin P, Fish J, Phelan P and Keblinski P 2006 *Appl. Phys. Lett.* **89** 143119
26. Charkraborty S and Padhy S 2008 *ACS Nano* **2** 2029
27. Rubio-Hernández F J, Ayúcar-Rubio M F, Vlaázquez-Navarro J F and Galindo-Rosales F J 2006 *J. Colloid Interface Sci.* **298** 967
28. Sarojini K G K, Manoj S V, Singh P K, Pradeep T and Das S K 2013 *Colloids Surf. A: Physicochem. Eng. Asp.* **417** 39
29. Ganguly S, Sikdar S and Basu S 2009 *Powder Technol.* **196** 326
30. Modesto-lopez L B and Biswas P 2010 *J. Aerosol Sci.* **41** 790
31. Baby T T and Ramaprabhu S 2010 *J. Appl. Phys.* **108** 124308
32. Glory J, Bonetti M, Helezen M, Mayne-L'Hermite M and Reynaud C 2008 *J. Appl. Phys.* **103** 094309
33. Cruz R C D, Reinshagen J, Oberacker R, Segadães A M and Hoffmann M J 2005 *J. Colloid Interface Sci.* **286** 579
34. Maxwell J C 1873 *Electricity and magnetism* (Oxford: Clarendon Press)
35. Ohshima H 2003 *Colloids Surf. A: Physicochem. Eng. Asp.* **222** 207
36. White S B, Shih A J and Pipe K P 2011 *Nanoscale Res. Lett.* **6** 346
37. Nguyen C T, Roy G, Gauthier C and Galanis N 2007 *Appl. Therm. Eng.* **27** 1501

38. Ma H B, Wilson C, Borgmeyer B, Park K and Yu Q 2006 *Appl. Phys. Lett.* **88** 1
39. Nguyen C T, Roy G, Lajoie P R and Maiga S E B 2005 *Proceedings of 3rd IASME/WSEAS international conference on heat transfer, thermal engineering and environment* (Greece: Corfu) pp. 160–165
40. Andablo-Reyes E, Hidalgo-Álvarez R and Vicente J 2011 *Soft Matter* **7** 880
41. Yao G Z, Yap F F, Chen G, Li W H and Yeo S H 2002 *Mechatronics* **12** 963
42. Xiang-Qi W and Arun S M 2008 *Brazilian J. Chem. Eng.* **24** 631
43. Jain P, El-Sayed I and El-Sayed M 2007 *Nano Today* **2** 18
44. Sun X *et al* 2008 *Nano Res.* **1** 203
45. Pankhurst Q A, Connolly J, Jones S K and Dobson J 2003 *J. Phys. D: Appl. Phys.* **36** R167
46. Gupta A K and Gupta M 2005 *Biomaterials* **26** 3995
47. Xie H, Yu W and Chen W 2010 *J. Exp. Nanosci.* **5** 463
48. Esfe M H, Saedodin S, Bahiraei M, Toghraie D, Mahian O and Wongwises S 2014 *J. Therm. Anal. Calorim.* (Springer) p. 287
49. Adio S A, Sharifpur M and Meyer J P 2015 *Heat Transf. Eng.* **36** 1241
50. Timofeeva E V *et al* 2007 *Phys. Rev. E* **76** 1
51. Wong K-F V and Kurma T 2008 *Nanotechnology* **19** 345702
52. Li Y, Zhou J, Tung S, Schneider E and Xi S 2009 *Powder Technol.* **196** 89
53. Mastuli M S, Ansari N S, Nawawi M A and Mahat A M 2012 *APCBEE Procedia* **3** 93
54. Suryanarayana C and Norton M G 1998 *X-ray diffraction: A practical approach* (New York: Plenum Press)
55. Samal S, Satpati B and Chaira D 2010 *J. Alloys Compd.* **504** S389
56. Kathrein H and Freund F 1983 *J. Phys. Chem. Solids* **44** 177
57. Wilson I O 1981 *IEE Proc. A: Phys. Sci. Meas. Instrum. Manage Educ. Rev.* **128** 159
58. Posner J D 2009 *Mech. Res. Commun.* **36** 22
59. Carrique F, Ruiz-reina E, Arroyo F J and Delgado V 2006 *J. Phys. Chem.* **B110** 18313
60. Minea A A and Luciu R S 2012 *Microfluid. Nanofluid.* **13** 977
61. Turner J 1976 *Chem. Eng. Sci.* **31** 487
62. Ram R, Gonz R, Chen Y and Alves E 2002 *Nucl. Instr. Meth. Phys.* **B191** 191
63. Ohshima H 2000 *J. Colloid Interface Sci.* **229** 307
64. Ohshima H 1999 *J. Colloid Interface Sci.* **212** 443
65. Ding J M and Keh H J 2001 *J. Colloid Interface Sci.* **236** 180
66. Kuwabara S 1959 *J. Phys. Soc. Japan* **14** 527
67. Ruiz-reina E 2007 *J. Phys. Chem.* **C111** 141